Article

Probing the Interior of Peptide Amphiphile Supramolecular Aggregates

John D. Tovar, Randal C. Claussen, and Samuel I. Stupp

J. Am. Chem. Soc., **2005**, 127 (20), 7337-7345• DOI: 10.1021/ja043764d • Publication Date (Web): 30 April 2005

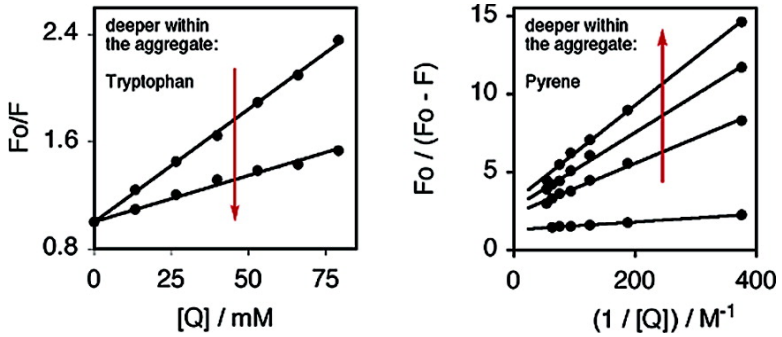

More About This Article

Additional resources and features associated with this article are available within the HTML version:

- Supporting Information
- Links to the 11 articles that cite this article, as of the time of this article download
- Access to high resolution figures
- Links to articles and content related to this article
- Copyright permission to reproduce figures and/or text from this article

View the Full Text HTML

J|A|C|S
ARTICLES
Published on Web 04/30/2005

Probing the Interior of Peptide Amphiphile Supramolecular Aggregates

John D. Tovar,[†,‡] Randal C. Claussen,[§] and Samuel I. Stupp*[,†,‡,§,||]

Contribution from the Department of Materials Science and Engineering, Institute for BioNanotechnology in Medicine (IBNAM), Department of Chemistry, and Feinberg School of Medicine, Northwestern University, Evanston, Illinois 60208

Received October 13, 2004; Revised Manuscript Received March 29, 2005; E-mail: s-stupp@northwestern.edu

Abstract: We present a study of the aqueous solvation within self-assembled structures formed from peptide amphiphiles. We have placed tryptophan and pyrene chromophores onto the peptide backbone to enable spectroscopic examinations of the interior of the resulting supramolecular objects. Self-assembly constrains the chromophores to a defined location within an aggregate, and they experience differing degrees of quencher penetration reflective of their depth within the nanostructure. Tryptophan fluorescence indicates that the interiors remain well-solvated, suggesting that the supramolecular aggregates maintain high degrees of free volume. The Stern−Volmer quenching constants and the fractional accessibility (of covalently bound pyrene) progressively increase as the chromophore is placed closer to the aggregate exterior. Furthermore, these aggregates encourage chromophore uptake from aqueous solution as evidenced by the solubilization of free pyrene chromophores. Our findings demonstrate that covalently bound fluorophores within an aggregate can interact with the external environment. Studies with small molecular probes indicate that these self-assembled architectures may represent viable vehicles to sequester hydrophobic, insoluble organic molecules (within the interior) and to present signaling protein epitopes to cells (on the periphery).

The self-assembly of biocompatible molecules into well-defined supramolecular objects has important implications for future medical applications seeking to use cellular signaling for tissue regeneration or to target the transport of small drugs and proteins. Inspired by biology, synthetic chemists have endeavored to create relatively simple molecular systems that assemble with proteinlike fidelity into predictable supramolecular constructs.[1] Key design elements (such as hydrogen bonding, van der Waals and Coulombic interactions, and solvent effects) have led to the realization of challenging synthetic targets ranging from "incarcerated" high-energy organic intermediates to well-defined lamellar sheets, micelles, and other supramolecular structures from molecularly designed precursors.[2] This diversity of molecular architectures enables preprogrammed assembly of complex structures with dimensions on the order of tens to hundreds of nanometers, size regimes not easily obtained through synthetic chemistry or current state-of-the-art lithography.

Aggregate formation between small synthetic peptides can model the buildup of β-amyloid plaques implicated in many neurodegenerative diseases. The very mechanism postulated for plaque formation has also enabled the construction of novel biomaterials. Zhang's charged oligopeptides formed β-sheets that ultimately collapsed into robust membranes.[3] Boden and colleagues found that small oligopeptides underwent a hierarchical assembly process leading to nematic hydrogels.[4] In both cases, the formation of β-sheet tapes from a well-defined peptide sequence initiated higher-order assembly into ribbons, fibrils, and fibers. Nowick and Kelly have designed elegant molecules with predisposed conformations that facilitate artificial β-sheet assembly.[5] Schneider and colleagues have designed soluble peptides where *reversible* intramolecular folding into β-sheetlike structures leads to distinct changes in macroscopic materials properties.[6] However, functional peptide materials need not rely solely on β-sheet morphologies as evidenced by D. Tirrell's reversible hydrogels from recombinantly synthesized triblock polypeptides and Deming's peptidic block copolymers.[7,8]

[†] Department of Materials Science and Engineering.
[‡] Institute for BioNanotechnology in Medicine (IBNAM).
[§] Department of Chemistry.
[||] Feinberg School of Medicine.

(1) *Comprehensive Supramolecular Chemistry*; Atwood, J. L., Davies, J. E. D., MacNicol, D. D., Vögtle, F., Eds.; Pergamon (Elsevier Science Inc.): New York, 1996.
(2) (a) Warmuth, R. *Angew. Chem., Int. Ed. Engl.* **1997**, *36*, 1347−1350. (b) Stupp, S. I.; LeBonheur, V.; Walker, K.; Li, L. S.; Huggins, K. E.; Keser, M.; Amstutz, A. *Science* **1997**, *276*, 384−389. (c) Stupp, S. I.; Pralle, M. U.; Tew, G. N.; Li, L.; Sayar, M.; Zubarev, E. R. *MRS Bull.* **2000**, *4*, 42−48.
(3) Zhang, S.; Holmes, T.; Lockshin, C.; Rich, A. *Proc. Natl. Acad. Sci. U.S.A.* **1993**, *90*, 3334−3338.
(4) (a) Aggeli, A.; Bell, M.; Boden, N.; Keen, J. N.; Knowles, P. F.; McLeish, T. C. B.; Pitkeathly, M.; Radford, S. E. *Nature* **1997**, *386*, 259−262. (b) Aggeli, A.; Bell, M.; Boden, N.; Carrick, L. M.; Strong, A. E. *Angew. Chem., Int. Ed.* **2003**, *42*, 5603−5606.
(5) (a) Holmes, D. L.; Smith, E. M.; Nowick, J. S. *J. Am. Chem. Soc.* **1997**, *119*, 7665−7669. (b) Lashuel, H. A.; LaBrenz, S. R.; Woo, L.; Serpell, L. C.; Kelly, J. W. *J. Am. Chem. Soc.* **2000**, *122*, 5262−5277.
(6) Schneider, J. P.; Pochan, D. J.; Ozbas, B.; Rajagopal, K.; Pakstis, L.; Kretsinger, J. *J. Am. Chem. Soc.* **2002**, *124*, 15030−15037.
(7) Petka, W. A.; Harden, J. L.; McGrath, K. P.; Wirtz, D.; Tirrell, D. A. *Science* **1998**, *281*, 389−392.
(8) (a) Deming, T. J. *Nature* **1997**, *390*, 386-390. (b) Euliss, L. E.; Grancharov, S. G.; O'Brien, S.; Deming, T. J.; Stucky, G. D.; Murray, C. B.; Held, G. A. *Nano Lett.* **2003**, *3*, 1489−1493. (c) Bellomo, E. G.; Wyrsta, M. D.; Pakstis, L.; Pochan, D. J.; Deming, T. J. *Nature Mater.* **2004**, *3*, 244−248.

Peptide amphiphiles (PAs) comprise one newer class of self-assembling molecules bearing hydrophilic peptide segments covalently coupled to lipid tails. These molecules take advantage of peptide secondary structure, and they draw parallels to phospholipids and other membrane-forming amphiphiles. Yamada designed charged amphiphiles consisting of a branched alkane tail, a tripeptide unit, and an ammonium salt that formed reversed cylindrical micelles in nonpolar organic solvents.[9] The double-branched amphiphiles studied by Yager and Gelb formed tubular microstructures 500 nm in diameter.[10] M. Tirrell has also studied peptide amphiphiles that form triple helical structures in monolayers at the air−water interface.[11] Thus, peptide amphiphiles present viable molecular precursors to a variety of supramolecular structures from individual fiberlike micelles to larger fibrillar aggregates and membrane mimics.

The authors' laboratory recently reported the first PAs that formed cylindrical objects in aqueous media. These molecules contain hydrophilic oligopeptide sequences *N*-acylated with palmitic acid.[12] Ionizable amino acids in the oligopeptide segments impart pH sensitivity to the molecules that ultimately drives self-assembly through hydrophobic collapse into high aspect ratio cylindrical nanostructures with diameters that scale with the dimensions of the molecular components (6−8 nm). Secondary β-sheetlike structure promoted by repeated residues such as alanine, leucine, and valine helps to stabilize the aggregates and, more importantly, leads to nanostructures with a high degree of order. This aspect differentiates them from cylindrical micelles formed by ordinary surfactants and block copolymers that essentially have an amorphous internal structure. These one-dimensional objects have excellent gelation properties, affording self-supporting hydrogels at low concentrations (0.1−1 wt % in water). Unlike earlier studies of self-assembling oligopeptides, these PAs consistently produce discrete cylindrical nanostructures from a large diversity of bioactive peptide sequences. We have recently used molecularly designed PAs to direct the mineralization of the bone material hydroxyapatite and to direct the differentiation of neural progenitor cells into neurons.[12a,13]

Geometric packing considerations can often help to predict a supramolecular structure expected from a self-assembling molecule such as an ionic surfactant.[14] However, our PA molecules exhibit an almost exclusive preference for assembly into cylindrical nanostructures. Analysis and prediction of this self-assembly requires careful consideration of intermolecular interactions such as hydrogen bonding and electrostatics. In efforts to better understand PA assembly on a molecular level, we have shown that the formation of β-sheetlike hydrogen-bonding motifs among PA molecules plays a significant role in the formation and stabilization of supramolecular aggregates.[15] Recent theoretical work has corroborated the importance of strong intermolecular interactions relevant to the collapse into cylindrical fiber morphologies after changes in pH or ionic strength screen charges and reduce electrostatic repulsion among molecules.[16] These nanostructures present ordered and directional interactions between molecular components that ultimately yield cylindrical structures rather than disordered spherical micelles. They can present bioactive epitopes to the aqueous environment while burying their fatty acid tails within the core of the aggregate.

Fluorescence techniques offer powerful tools to examine the structure and dynamics of macromolecular systems. Structural studies of protein macromolecular architecture often take advantage of tryptophan's environmentally sensitive emission wavelength. Tryptophan presents structured, high-energy emission profiles in hydrophobic environments as exemplified by the 315-nm emission maximum when buried in the hydrophobic pocket of the protein azurin. In contrast, proteins such as glucagon, where tryptophan has greater exposure to water, display broad red-shifted fluorescence at 355 nm.[17] In most cases, the nature of the solvation sphere directly correlates to the accessibility of an aqueous fluorescence quencher. For example, the buried tryptophan within the hydrophobic pocket of azurin displays a ca. 74-fold lower quenching rate in the presence of acrylamide relative to glucagon's exposed tryptophan.[18]

Synthetic self-assembling systems have also validated the use of fluorescent molecules as supramolecular probes. Beddard and colleagues have employed tryptophan to study the energy migration that occurs through π-stacked electronic conduits within self-assembled oligopeptide ribbon nanostructures.[19] Time-resolved measurements of tryptophan-tagged model systems have also revealed the dynamics of collagen assembly.[20] Other studies have taken advantage of the intense fluorescence and unique excimer-forming properties of pyrene, a probe of choice to study membrane fluidity and cellular uptake of synthetic materials.[21] Pyrene and related fluorescent derivatives provide convenient spectroscopic handles to probe the conformations of polymers and dendrimers[22] and to model the controlled release of hydrophobic molecules from polymer micelles and other drug-delivery vehicles.[23]

To fully realize drug or protein carrier capabilities and biological signaling applications for peptide amphiphile supramolecular constructs, it is important to determine the nature of the aggregate's interior and assess the ability for small

(9) (a) Yamada, N.; Koyama, E.; Imai, T.; Matsubara, K.; Ishida, S. *Chem. Commun.* **1996**, 2297−2298. (b) Yamada, N.; Ariga, K.; Naito, M.; Matsubara, K.; Koyama, E. *J. Am. Chem. Soc.* **1998**, *120*, 12192−12199.
(10) Lee, K. C.; Carlson, P. A.; Goldstein, A. S.; Yager, P.; Gelb, M. H. *Langmuir* **1999**, *15*, 5500−5508.
(11) (a) Berndt, P.; Fields, G. B.; Tirrell, M. *J. Am. Chem. Soc.* **1995**, *117*, 9151−9522. (b) Yu, Y.-C.; Berndt, P.; Tirrell, M.; Fields, G. B. *J. Am. Chem. Soc.* **1996**, *118*, 12515−12520.
(12) (a) Hartgerink, J. D.; Beniash, E.; Stupp, S. I. *Science* **2001**, *294*, 1684−1688. (b) Hartgerink, J. D.; Beniash, E.; Stupp, S. I. *Proc. Natl. Acad. Sci. U.S.A.* **2002**, *99*, 5133−5138.
(13) Silva, G. A.; Czeisler, C.; Niece, K. L.; Beniash, E.; Harrington, D. A.; Kessler, J. A.; Stupp, S. I. *Science* **2004**, *303*, 1352−1355.
(14) Israelachvili, J. N. *Intermolecular and Surface Forces*, 2nd ed.; Academic Press: San Diego, 1992.
(15) Behanna, H. A.; Donners, J. J. J. M.; Gordon, A. C.; Stupp, S. I. *J. Am. Chem. Soc.* **2005**, *127*, 1193−1200.
(16) Tsonchev, S.; Troisi, A.; Schatz, G. C.; Ratner, M. A. *Nano Lett.* **2004**, *4*, 427−431.
(17) Lakowicz, J. *Principles of Fluorescence Spectroscopy*, 2nd ed.; Kluwer Academic/Plenum: New York, 1999; Chapter 16.
(18) (a) Eftink, M. R.; Ghiron, C. A. *J. Phys. Chem.* **1976**, *80*, 486-493. (b) Eftink, M. R.; Ghiron, C. A. *Biochemistry* **1976**, *15*, 672−680. (c) Eftink, M. R.; Ghiron, C. A. *Biochemistry* **1977**, *16*, 5546−5551.
(19) Kayser, V.; Turton, D. A.; Aggeli, A.; Beevers, A.; Reid, G. D.; Beddard, G. S. *J. Am. Chem. Soc.* **2004**, *126*, 336−343.
(20) Simon-Lukasik, K. V.; Persikov, A. V.; Brodsky, B.; Ramshaw, J. A. M.; Laws, W. R.; Ross, J. B. A.; Ludescher, R. D. *Biophys. J.* **2003**, *84*, 501−508.
(21) (a) Pownall, H. J.; Smith, L. C. *Chem. Phys. Lipids* **1989**, *50*, 191−211. (b) Barenholz, Y.; Cohen, *J. Biol. Chem.* **1996**, *271*, 3085−3090.
(22) (a) Winnik, F. M.; Winnik, M. A.; Tazuke, S.; Ober, C. K. *Macromolecules* **1987**, *20*, 38−44. (b) Frank, R. S.; Merkle, G.; Gauthier, M. *Macromolecules* **1997**, *30*, 5397−5402. (c) Cardona, C. M.; Wilkes, T.; Ong, W.; Kaifer, A. E.; Donovan McCarley, T.; Pandey, S.; Baker, G. A.; Kane, M. N.; Baker, S. N.; Bright, F. V. *J. Phys. Chem. B.* **2002**, *106*, 8649−8656.
(23) (a) Liu, M.; Kono, K.; Fréchet, J. M. J. *J. Control. Release* **2000**, *65*, 121−131. (b) Lele, B. S.; Leroux, J.-C. *Macromolecules* **2002**, *35*, 6714−6723. (c) Paleoa, C. M.; Tsiourvas, D.; Sideratou, Z.; Tziveleka, L. *Biomacromolecules* **2004**, *5*, 524−529.

Chart 1. Chemical Structures of the PAs Studied in This Report

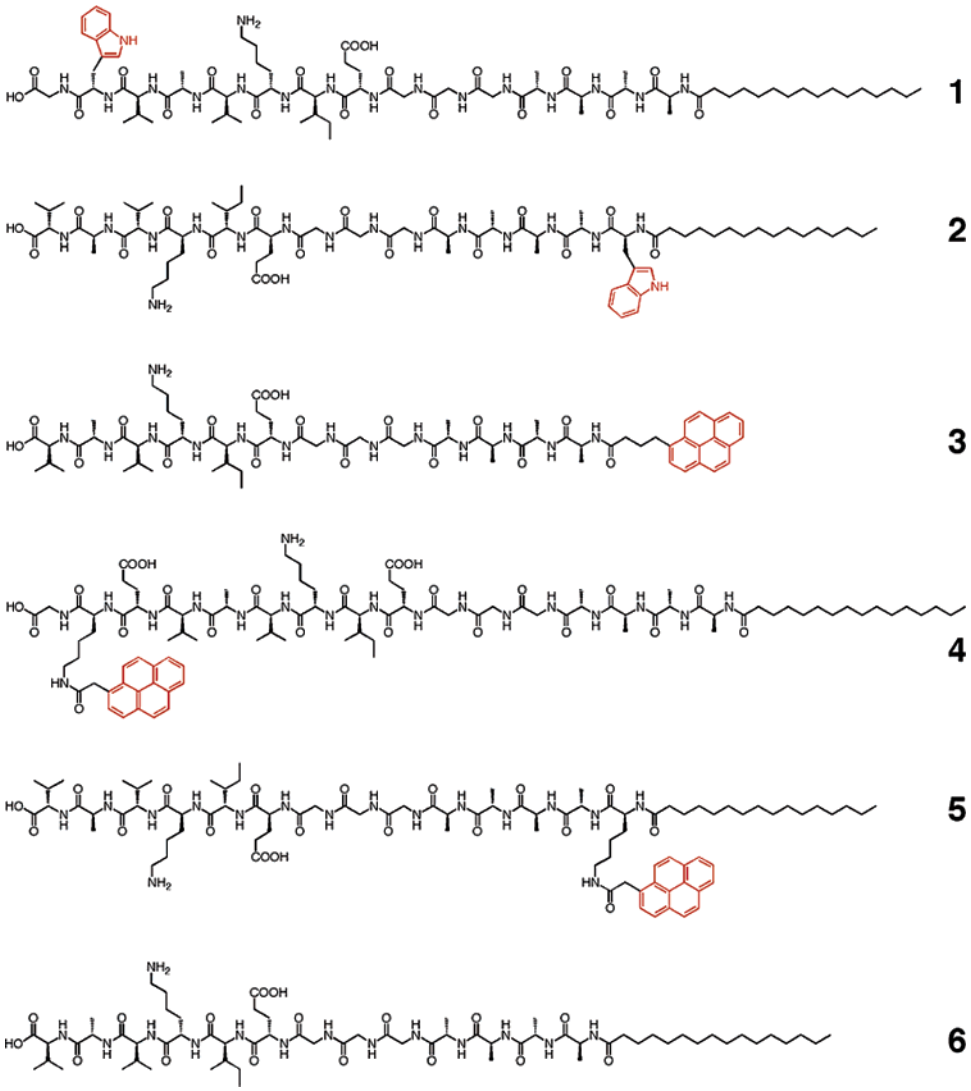

molecules to enter the assembled nanostructure. We describe here the synthesis of PAs bearing fluorophores at specific locations along the peptide backbone. Self-assembly driven by low pH should place these chromophores in defined environments that experience differing degrees of solvent exposure and quencher accessibility. Steady-state fluorescence data illustrates the extent of solvation once the chromophores are embedded within the self-assembled structures. Stern−Volmer analysis of fluorescence intensity changes that accompany the addition of aqueous acrylamide (a fluorescence quenching agent) should reveal the extent of small molecule access within the nanostructures. We also study here the sequestration of free pyrene fluorophores within the cylindrical nanostructures. These studies will provide helpful information to assess the use of supramolecular objects to carry hydrophobic, water-insoluble molecules for applications in drug delivery. This same ability simultaneously offers promise for examining confined polymerizations of hydrophobic monomers sequestered within PA nanostructures.

Results and Discussion

Peptide Amphiphile Design Considerations. Chart 1 depicts five fluorophore-containing PAs used in the current study (**1**−**5**), along with a nonfluorescent control PA (**6**) studied previously.[13] We anticipated that these specific peptide sequences would allow for spatial control of the fluorescent reporter group within a supramolecular aggregate. All fluorescent sequences maintain structural similarity to the control PA, enabling the formation of mixed nanostructures containing diluted fluorescent probes for spectroscopic studies. The IKVAV pentapeptide mimics laminin sequences known to foster integrin binding in a number of cell types,[24] while the tetra(alanine) segment promotes β-sheet formation between PA molecules.[12b]

PAs **1** and **2** incorporate a tryptophan residue at two extremes of the peptide segment. Assembly driven by low pH will lead to two spectroscopically distinct PA aggregates as illustrated in Chart 2. The tryptophans in an aggregate composed of PA **1** present themselves closer to the outer shell and should display spectroscopic signatures reminiscent of a well-solvated tryptophan in a hydrophilic environment (Chart 2A). In contrast, the assembly of PA **2** should place the tryptophans deeper within the self-assembled structure (Chart 2B). We should observe a blue-shifted fluorescence a priori if pH-driven collapse of these molecules indeed leads to the formation of a hydrophobic

(24) Tashiro, K.; Sephel, G. C.; Weeks, B.; Sasaki, M.; Martin, G. R.; Kleinman, H. K.; Yamada, Y. *J. Biol. Chem.* **1989**, *264*, 16174−16182.

Chart 2 [a]

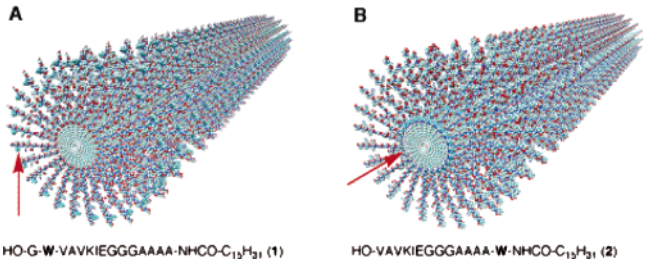

[a] Red arrows indicate the tryptophan residues once the respective PA molecules have self-assembled.

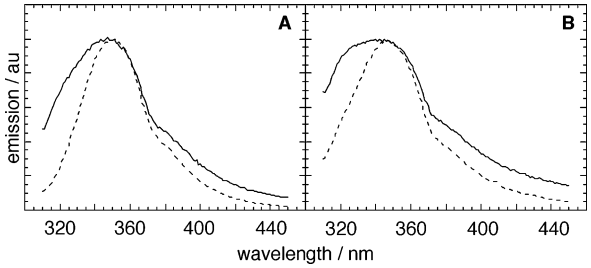

Figure 1. Normalized, representative fluorescence emission of (A) PA **1** and (B) PA **2** after excitation at 290 nm under basic (dashed line) and acidic (solid line) conditions.

interior. Chromophores closer to the exterior of the aggregate should also have greater interactions with soluble quenching agents.

PAs **3**, **4**, and **5** have covalent pyrene labels. Pyrene-tagged PA **3** offers one extreme whereby self-assembly should sequester all pyrene chromophores within the hydrophobic core, while amidation of the appropriate lysine ϵ-amine of PAs **4** and **5** places the pyrene group in locations comparable to the tryptophans of **1** and **2** above. Pyrene displays a significantly higher quantum yield compared to tryptophan, facilitating spectroscopy of coassembled nanostructures comprised primarily with the nonfluorescent IVKAV PA **6**. Chromophore dilution will minimize any complications that may arise from interchromophore interactions in the assembled aggregates.

Synthesis of Peptide Amphiphiles. We utilized standard fluorenylmethoxycarbonyl (Fmoc)-protected solid-phase automated synthesis to construct peptide segments on preloaded Wang resin supports followed by manual *N*-acylation with palmitic acid (or 1-pyrene butyric acid in the case of **3**). Orthogonal lysine protecting groups allowed for the selective unveiling of a particular ϵ-amine on the immobilized peptide as a means to install pyrene into PAs **4** and **5** via acylation with pyrene acetic acid. We preventatively added ethanedithiol (EDT) to our cleavage solutions (94% CF_3COOH, 2% *i*-Pr_3-SiH, 2% H_2O, 2% EDT) to suppress undesired intramolecular cyclization between the indole ring of tryptophan and the adjacent peptide backbone,[25] a side reaction known to yield highly colored trace impurities.

Verification of Peptide Amphiphile Assembly. Basic solutions of PAs **1**−**5** (ca. pH 10) formed self-supporting gels following the slow diffusion of acid vapor (HCl), suggestive of the formation of networked one-dimensional objects. Similarly, mixed solutions of PA **6** with either **3**, **4**, or **5** (in a 40:1 ratio) yielded highly transparent self-supporting gels upon diffusive acidification. We have empirically found that the formation of a self-supporting PA hydrogel offers strong evidence for the presence of high aspect ratio 1-D objects and networked aggregates thereof. Transmission electron microscopy verified the presence of 1-D aggregate structures in bulk samples of all PAs studied (Supporting Information). Circular dichroism measurements on basic solutions of PAs **1** and **2** revealed characteristic β-sheetlike signatures (Supporting Information) and concentrated (ca. 10 mg/mL) solutions of PAs **1**−**3** at basic pH formed gels over a period of several minutes. We take these observations as evidence that the PA molecules already interact to some extent at basic pH. However, lower pH increases the rate of hydrophobic collapse into larger aggregates by screening electrostatic repulsion between molecules. We have shown that β-sheet formation typically accompanies the supramolecular aggregation of PAs in dilute solution regardless of the specific conditions required to trigger assembly or the conformation of the unassembled molecules at basic pH.[15] With a given PA sequence, we can reasonably equate the pH of a solution to a dominant supramolecular morphology even at concentrations too low to create a self-supporting hydrogel. This will factor into photophysical studies that require optically isotropic and highly dilute solutions.

Steady-State Tryptophan Fluorescence. We studied the steady-state emission profiles of tryptophan PAs **1** and **2** to understand the solvation within the cylindrical aggregates that form from these molecules upon acidification and subsequent hydrophobic collapse. We prepared our spectroscopic solutions at concentrations sufficiently high to observe meaningful fluorescence while dilute enough to minimize extensive scattering from visible aggregates.[26] In basic solution, PAs **1** and **2** display spectroscopic profiles consistent with fully solvated tryptophan moieties: PA **1** shows the characteristic indole absorption at 281 nm with an emission maximum at 350 nm (Figure 1A, dashed line), while PA **2** absorbs at 283 nm and emits at 346 nm (Figure 1B, dashed line). Upon acidification (and assembly), we observe a subtle blue shift of the peak fluorescence intensities for both PAs **1** (346 nm, Figure 1A, solid line) and **2** (342 nm, Figure 1B, solid line). For comparison, the small tryptophan molecule *N*-acetyltryptophanamide (NATA) emits at 356 nm under identical basic and acidic conditions.

Under the acidic conditions that drive assembly, PAs **1** and **2** show pronounced high-energy shoulders at 325 nm, although those observed for PA **2** were consistently stronger than those observed for **1**. While these shifts in peak intensities are not as dramatic as those observed between hydrophobic extremes of protein environments, they suggest a slight increase in hydrophobicity around the tryptophans upon self-assembly, regardless of their placement along the peptide. However, these residues remained well solvated after assembly compared to more hydrophobic protein environments such as those present in the azurins. This supports an idea of directional β-sheet structures between PA molecules existing throughout the assembled aggregates, leaving void spaces between collapsed sheets within the nanostructure. Such extensive solvation suggests that aqueous small molecules may also experience unrestricted access within the aggregate.

(25) Sugimoto, H.; Nakanishi, E.; Hibi, S. *Polymer* **1998**, *39*, 5739−5745.

(26) For a discussion of experimental issues relevant to the measurement of tryptophan's photophysical behavior, see: Ladokhin, A. S.; Jayasinghe, S.; White, S. H. *Anal. Biochem.* **2000**, *285*, 235−245.

Table 1. Rates of Quenching Determined from Stern−Volmer Analysis[a]

	k_{SV}/M^{-1}	$\langle\tau_0\rangle$/ns	$k_Q/10^9\ M^{-1}\ s^{-1}$
1 (basic)	39.0	2.7	14
1 (acidic)	16.8	1.8	9.3
2 (basic)	17.5	3.0	5.8
2 (acidic)	7.81	3.3	2.4
NATA (basic)	42.3	2.7	16
NATA (acidic)	32.2	2.2	15

[a] Basic solutions had pH values ca. 10 while acidic solutions had pH values ca. 2.

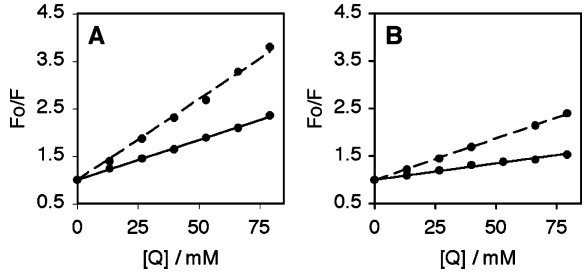

Figure 2. Representative Stern−Volmer quenching plots for (A) PA **1** and (B) PA **2** under basic (dashed line) and acidic (solid line) conditions. Q = acrylamide.

Stern−Volmer Quenching Analysis. Fluorescence quenching experiments can quantitate the degree of solvent exposure at specific sites of a protein. For example, the quenching response of tryptophan mutant proteins in the presence of the electron-transfer agent acrylamide has served as a powerful probe of the chromophore's local environment.[27] Unlike ionic quenching agents such as iodide salts, neutral acrylamide does not interact electrostatically with charged molecules, making it ideal to probe our solvated, charged PAs and their self-assembled, less charged counterparts. We conducted systematic Stern−Volmer studies under basic, nonassembling conditions and under the acidic conditions that foster self-assembly into cylindrical aggregates for all of the fluorescent PAs depicted in Chart 1. For dynamic bimolecular collisional quenching, eq 1 describes the ideal Stern−Volmer relation between quencher concentration and fluorescence intensity

$$F_0/F = 1 + k_{SV}[Q] = 1 + k_Q\tau_0[Q] \qquad (1)$$

Where F represents the fluorescence intensity at a given quencher concentration [Q], F_0 represents the initial fluorescence intensity in the absence of quencher and k_{SV} represents the Stern−Volmer constant. Furthermore, the k_{SV} term represents a product of the initial fluorescence lifetime (τ_0) and the bimolecular quenching rate constant (k_Q). By experimental measurement of F_0, F as a function of [Q], and τ_0, we can relate k_Q values for a given molecule to the environment it's chromophore experiences both before and after self-assembly.

Quenching of Tryptophan Fluorescence. Basic solutions of **1** and **2** display steeper Stern−Volmer slopes, indicative of greater quenching relative to their assembled, acidic counterparts (Table 1 and Figure 2). We observe the quencher access to decrease within the assembled structures of PA **1** and **2** by a factor of 2.3 and 2.2, respectively (parts A and B of Figure 2). We stress that these data represent typical results rather than absolute values as the magnitude of these quenching data varied despite careful attempts to replicate sample preparation. The spectroscopic solutions consisted of polydisperse aggregates with differing degrees of light scattering; however, we observed consistent *trends* among all of our samples. Notably, PA **2**, which should place the tryptophan moiety deeper within the self-assembled structure, has a 2-fold lower k_{SV} compared to the value obtained from aggregates with peripheral tryptophans found in assembled structures of PA **1**. We also measured comparable k_{SV} values for the assembled PA **1** and the *unassembled* PA **2** and attribute this to differing degrees of pre-existing interactions between the two PA systems before acid-induced assembly, as discussed above. We conclude that the self-assembled aggregates, while relatively well-solvated (vide supra), slightly restrict access to the external environment. These data also confirm that the supramolecular environment will allow for the penetration of molecular analytes within the interior of the cylindrical nanostructure, serving to facilitate ongoing studies that require small molecule diffusion within the self-assembled structures.

We corrected the Stern−Volmer data to account for differences in fluorescence lifetimes between PAs **1** and **2** in the absence of quenchers (see eq 1). We used weighted averages of the measured lifetime components since phase-modulated lifetime measurements revealed multiexponential decays. Even in proteins with single tryptophan chromophores situated in well-defined locations, complex multiexponential fluorescence decays often exist.[28] In our systems, the inherently polydisperse nature of the aggregates complicated the lifetime measurements. Tryptophan-mediated energy transfer may also play a role within the self-assembled aggregates as discussed by Beddard.[19]

We find that the trends in k_{SV} observed between assembled structures formed by PAs **1** and **2** are consistent with those found in k_Q, with assembled PA **1** displaying a k_Q value almost 4-fold greater than that for assembled PA **2** (Table 1). For comparison, the nonassembling NATA displays comparable k_Q values in acidic and basic media. The relatively high values of k_Q observed in the assembled aggregates of PAs **1** and **2** would suggest that these aggregates do indeed maintain high degrees of free volume and solvation presumably arising from less dense packing upon hydrophobic collapse allowing for greater solvation within the nanostructures, corroborating the steady-state fluorescence data presented above (Figure 1). We attempted to probe isolated tryptophan PAs randomly coassembled within nanostructures derived from IKVAV PA **6** in order to eliminate electronic perturbations among tryptophans. Unfortunately, we could not obtain meaningful fluorescence data from these coassembled structures due to inherently weak tryptophanyl fluorescence signals coupled with extensive formation of large aggregates after assembly. The pyrene systems discussed below helped to resolve these complications.

Steady-State Pyrene Fluorescence. Pyrene-tagged PA **3** allowed us to observe the quenching behavior in a much more hydrophobic environment relative to both tryptophan PAs presented above. While pyrene does not possess the environmentally sensitive emission wavelength of tryptophan, it provides a much more intense signal thus minimizing the complicating effects from Raman scattering of water. We could also mimic the chromophore placement of the tryptophan

(27) Weber, J.; Senior, A. E. *Biochemistry* **2000**, *39*, 5287−5294.

(28) Nanda, V.; Liang, S.-M.; Brand, L. *Biochem. Biophys. Res. Commun.* **2000**, *279*, 770−778.

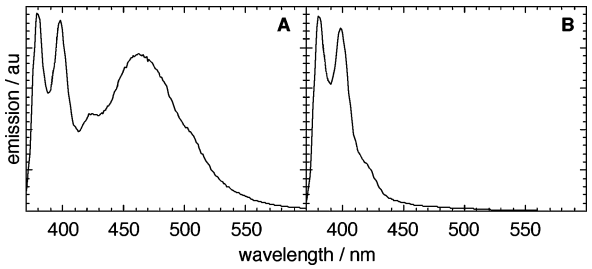

Figure 3. Steady-state fluorescence spectra of acidic solutions of (A) assembled PA **3** and (B) a mixed assembly of PAs **3** and **6** in a 1:40 ratio.

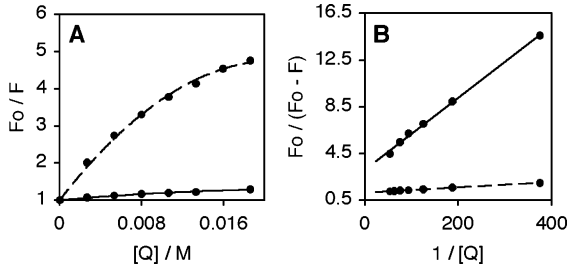

Figure 4. Stern−Volmer (A) and modified Stern−Volmer (B) treatments of quenching data from mixed PA solutions (1:40 **3**:**6**) at basic (dashed line) and acidic (solid line) pH. Q = acrylamide.

systems with pyrene PAs **4** and **5**, both synthesized on solid supports using orthogonal protecting group strategies (see Experimental Section). The high quantum yield of pyrene relative to tryptophan allowed us to easily dilute the pyrenyl PAs within self-assembled structures through coassembly with the IKVAV PA **6**. This dilution essentially eliminated fluorescence contributions from the pyrene excimer known to form at higher concentrations.

Figure 3 clearly reveals the electronic perturbations resulting from π-stacking originating in the ground state and/or from excited-state excimer formation. Under self-assembling conditions (low pH), spectroscopic solutions of **3** yield a strong excimer emission (460 nm) along with the vibronic bands associated with isolated free monomer emission (380 and 400 nm). Coassembly in the presence of a 40-fold excess of **6** results in emission dominating from the free monomer. We have previously studied the electrostatic assembly PAs where oppositely charged amino acid residues facilitate assembly.[29] The systems at hand have similar charge, and we see no evidence for phase segregation among the two components, e.g., the lack of excimer emission in the 1:40 diluted case (Figure 3B). We have used this 1:40 dilution in all spectroscopic studies employing pyrene to assess the quenching behavior in the absence of competitive intermolecular decay pathways.

Quenching of Pyrene Fluorescence. We measured the quenching responses of the pyrene PAs under basic and acidic conditions as described for the tryptophan systems except with a 40-fold excess of the nonfluorescent IKVAV PA **6** to minimize intermolecular electronic interactions. Unlike PAs **1** and **2**, the Stern−Volmer responses of both the basic and the acidified solutions of coassembled PAs **3**, **4**, or **5** strongly deviated from linearity toward the *x*-axis at higher concentrations of acrylamide. This behavior indicates the presence of multiple fluorophore populations that display different responses to the added quencher, with one population considered completely shielded from the aqueous environment.[17] Modified Stern−Volmer treatments that account for differential accessibility provided more adequate fits to the observed quenching responses,[30] under the assumption that the assembled nanostructures contain a population of pyrene moieties completely inaccessible to aqueous quenchers. This convention provides an initial approximation that simplifies mathematical treatment and allows for extrapolation of the fraction of quencher-accessible chromophores (f_a) and the associated Stern−Volmer quenching constant of that population (k_a).[30]

Figure 4 illustrates the response of the 1:40 ratio of pyrene PA **3** to IKVAV PA **6** under basic (nonassembling) conditions and under acidic conditions that drive assembly. The marked deviation from linearity observed in the Stern−Volmer plot under basic conditions (Figure 4A) suggests interaction among the PA molecules even at high pH, but this behavior is not unprecedented (vide supra). Modified analysis of this quenching data (Figure 4B, dashed line) gives an f_a value of 87% and a k_a value of 521 M^{-1} under basic conditions. However, acidic pH dramatically enhances these interactions leading to extensive self-assembly, and the modified Stern−Volmer analysis yields an f_a value of 32%, with a k_a value of 101 M^{-1} (Figure 4B, solid line). This suggests that the pyrene moieties presumably buried within the hydrophobic alkyl core of the aggregate are significantly shielded from water, yet can still undergo quenching by aqueous agents. Unfortunately, we cannot compare this value directly to the k_Q values determined for the tryptophan PAs above. The multiexponential fluorescence lifetimes measured for the pyrene systems under acidic conditions correspond to the time decay of both solvent-exposed and buried chromophores. As we cannot correlate the lifetime of a particular component to the environment or location of the chromophore giving rise to that component, we can offer no quantitative comparisons with the tryptophan quenching rates or Stern−Volmer constants.

To investigate the relative magnitude of quencher accessibility within nanostructures where the pyrene chromophores lie at locations comparable to those found within the respective tryptophanyl PAs, we studied the pyrene-tagged PAs **4** and **5** after 40-fold dilution with the IKVAV PA **6**. Careful analysis of quenching behavior using modified Stern−Volmer formalisms revealed subtle yet consistent trends in the accessibility of quenchers with respect to their location on the self-assembling PA backbone. Figure 5 presents quenching for 1:40 dilutions of either **4** (A) or **5** (B) with the nonfluorescent **6** in both acidic and basic media. After consideration of the data presented in Figure 4, we find a trend toward decreased percentages of accessible chromophores and decreased Stern−Volmer constants with pyrene placement deeper within the assembled aggregate. Compared to the f_a value of 32% measured for the pyrene presented at the hydrophobic tail of PA **3**, we find an f_a value for **5** of 37% and an f_a value of 43% for **4**, where the pyrene

(29) Niece, K. L.; Hartgerink, J. D.; Donners, J. J. J. M.; Stupp, S. I. *J. Am. Chem. Soc.* **2003**, *125*, 7146−7147.

(30) Lehrer, S. S. *Biochemistry* **1971**, *10*, 3254−3263. Modified Stern−Volmer plots used herein take into consideration that only a fraction of a chromophore population will interact with the added quenching agent. In these plots, $F_0/(F_0 - F)$ is plotted vs 1/[Q] to yield a linear plot. From these data, the *y* intercept defines f_a^{-1} (where f_a is the fraction of accessible chromophores), and the intercept/slope value provides k_a, the apparent Stern−Volmer constant for the accessible chromophores. This analysis sets the Stern−Volmer constant for the inaccessible chromophores to zero as an initial estimation. In the present case, this assumption provides adequate fits to the experimental data, with no apparent need to consider nonzero values for the quenching response of other chromophore populations.

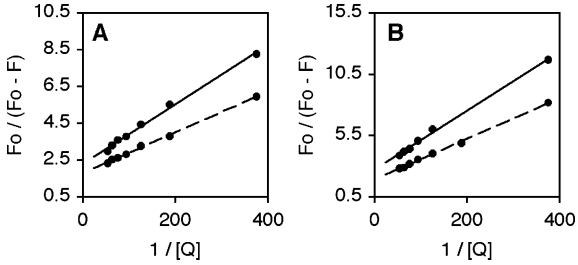

Figure 5. Modified Stern−Volmer analysis of quenching data from solutions of (A) **4** and (B) **5** in the presence of a 40-fold excess of **6** at basic (dashed line) and acidic (solid line) pH. Q = acrylamide.

Table 2. Pyrene Quenching Parameters Determined from Modified Stern−Volmer Analysis[a]

	f_a/%	k_a/M^{-1}	$\langle\tau_0\rangle$/ns[b]
3 (basic)	87	520	140
3 (acidic)	32	100	150
4 (basic)	56	160	180
4 (acidic)	43	140	150
5 (basic)	52	120	180
5 (acidic)	37	110	170
PAA (basic)[c]	100	710	110
PAA (acidic)[c]	77	520	120

[a] Basic solutions had pH values of ca. 10, while acidic solutions had pH values of ca. 2. All solutions prepared with a 40-fold molar excess of the nonfluorescent diluent **6**. [b] Lifetime values represent a weighted average of the observed multiexponential decays for all fluorescent chromophore populations. [c] PAA = pyrene acetic acid.

unit presumably rests closest to the exterior of the nanostructure. We also find that the apparent Stern−Volmer constant (k_a) increases as we progress from coassembled **3** to **5** to **4** (101 to 113 to 143 M^{-1}, respectively). The flexible four-carbon spacer of lysine offers greater conformational freedom to the pyrene probe, but nevertheless, these data mirror the expected proximity of the probe to the exterior of the aggregate. It suggests that the efficiency of diffusional quenching drops as the chromophore moves deeper within the self-assembled nanostructure. Although the data presented here allow us to calculate a finite f_a value for the respective nanostructures, we would expect that these "inaccessible" populations themselves would indeed undergo quenching at the extreme of higher acrylamide concentrations. Consistent with the tryptophan-quenching studies, we find that *all* accessible chromophore populations may interact with small molecule quenchers to different degrees despite their depth within the nanostructure. This offers the possibility that other small molecules will have similar access requisite for the use of PA nanostructures as delivery vehicles. Table 2 summarizes quenching data and lifetime measurements for the pyrene coassemblies.

Encapsulation of Molecular Chromophores: Microviscosity. The self-assembly of PAs into cylindrical nanostructures should create a dense hydrocarbon-like microenvironment within an aqueous gel. The environments created locally upon assembly of the fluorescent systems presented herein significantly retard, *but do not completely eliminate*, diffusion of aqueous quenchers. This property makes PA nanostructures and other self-assembling systems potentially ideal candidates for the delivery of hydrophobic or water-insoluble molecules in vivo. A variety of amphiphilic structures (block copolymers, anionic and cationic surfactants, etc.) can sequester hydrophobic or lipid-soluble organic molecules in aqueous solution during the self-assembly process.[31] This strategy has also found application in

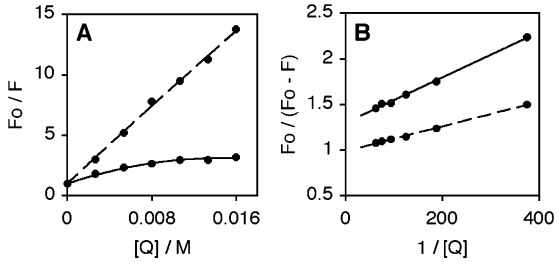

Figure 6. Stern−Volmer (A) and modified Stern−Volmer (B) treatments of quenching data from solutions of pyrene acetic acid in the presence of a 40-fold excess of PA **6** at basic (dashed line) and acidic (solid line) pH. Q = acrylamide.

the synthesis of conducting polymers.[32] Amphiphiles used for these studies typically have well-defined segments that impart a characteristic affinity for water, e.g., polyisoprene and poly(acrylic acid) for block copolymers, or ionic headgroups and alkyl tails for charged surfactants.

Peptide amphiphiles present a range of hydrophobicities within a given molecule. Molecules studied herein contain a hydrophilic, ionizable EIK sequence, an uncharged AAAAGGG sequence of intermediate hydrophobicity, and a lipidlike hydrophobic palmitoyl tail. We envisioned that Stern−Volmer studies would help to assess the location of a molecular fluorophore within the cylindrical aggregate after sequestration through a comparison to trends found for covalently tagged chromophore assemblies studied. To do so, we examined the behavior of pyrene acetic acid (a molecular pyrene chromophore) in the presence of a 40-fold excess of nonfluorescent PA **6** under both basic (nonassembling) and acidic (assembling) conditions.

In spectroscopic solutions at basic pH, we found linear Stern−Volmer behavior at the quencher concentrations employed in this study, as evidenced by the linear fits shown in Figure 6 (dashed lines). The *y* intercept of **1** found in the modified treatment further confirms complete chromophore accessibility (Figure 6B). This contrasts with the situation for solutions of pyrene PAs **3**−**5** at basic pH that showed nonlinear behavior at higher acrylamide concentrations. We speculate that this behavior reflects a stronger propensity for preassociation within the peptidic segments of the pyrene-tagged PAs **3**−**5**, even under basic conditions (vide supra). Despite apparent deprotonation, the free pyrene chromophore does not appreciably preassociate with the 40-fold excess of the PA diluent under the same basic conditions. Acidified spectroscopic solutions once again yielded negative nonlinear deviations in the Stern−Volmer behavior suggestive of chromophore populations with differing degrees of solvent exposure. The modified treatment could better quantitate this exposure, and we calculated an f_a value of 77% with an associated k_a value of 520 M^{-1}, much greater values

(31) (a) Gao, Z.; Lukyanov, A. N.; Singhal, A.; Torchilin, V. P. *Nano Lett.* **2002**, *2*, 979−982. (b) Soo, P. L.; Luo, L.; Maysinger, D.; Eisenberg, A. *Langmuir* **2002**, 18, 9996−10004. (c) Keyes-Beig, C.; Duhamel, J.; Fung, S.-Y.; Bezaire, J.; Chen, P. *J. Am. Chem. Soc.* **2004**, *126*, 7522−7532.

(32) Aniline: (a) Kuramoto, N.; Michaelson, J. C.; McEvoy, A. J.; Grätzel, M. *J. Chem. Soc., Chem. Commun.* **1990**, 1478−1480. (b) Österholm, J.-E.; Cao, Y.; Klavetter, F.; Smith, P. *Synth. Met.* **1993**, *55*−*57*, 1034−1039; Pyrrole: (c) Jang, J.; Yoon, H. *Chem. Commun.* **2003**, 720−721; EDOT: (d) Sakmeche, N.; Aaron, J. J.; Fall, M.; Aeiyach, S.; Jouini, M.; Lacroix, J. C.; Lacaze, P. C. *Chem. Commun.* **1996**, 2723−2724. Other templation strategies: (e) Hulvat, J. F.; Stupp, S. I. *Angew. Chem., Int. Ed.* **2003**, *42*, 778−781. (f) Hatano, T.; Bae, A.-H.; Takeuchi, M.; Fujita, N.; Kaneko, K.; Ihara, H.; Takafuji, M.; Shinkai, S. *Angew. Chem., Int. Ed.* **2004**, *43*, 465−469. (g) Carswell, A. D.; O'Rear, E. A.; Grady, B. P. *J. Am. Chem. Soc.* **2003**, *125*, 14793−17500.

than those found for the pyrene systems above. In the basic solution, pyrene acetic acid in the presence of 40-fold excess of **6** showed an apparent rate of quenching of 706 M^{-1} with all chromophores accessible. As pyrene acetic acid lacks peptidic structure, we would not expect it to associate with the IKVAV PA appreciably relative to peptidic fluorophores **3**−**5**, demonstrating the importance of hydrogen-bonding networks within the PA nanostructures.

We compared these responses to those observed for the same chromophore in solvents of varying viscosities. Aliquots of pyrene acetic acid dissolved in acidic glycerol/water solutions show a predictable decrease of k_{SV} (and k_Q) as the solution bulk viscosity increases. Increased viscosity will hinder diffusion of the aqueous quencher thereby minimizing collisional contact with the fluorophore during the lifetime of excited state and ultimately suppressing the k_{SV} relative to water. In all cases, we only considered the linear regimes of the standard Stern−Volmer plots, disregarding pseudostatic effects arising from the quenching sphere of action at higher quencher concentrations (i.e., positive deviations away from the *x* axis). We found that 10% glycerol solutions provided comparable k_a values to those found for pyrene acetic acid assembled in the presence of PA **6**. Spectroscopic solutions of assembled PAs had a bulk viscosity of 1.12 cP while the 10% glycerol solution had a viscosity of 1.26 cP as measured by a dropping-ball viscosimeter. For comparison, basic PA solutions had a viscosity of 1.09 cP, indicating that the dramatic decrease in quenching rate upon assembly reflects a change in viscosity at the nanoscale rather than a change in diffusional ability through the solution as a whole. It also suggests that the pyrene chromophores are dispersed throughout the peptide and lipid portions of the nanostructures rather than merely adsorbed to the surface of the self-assembled structure or freely soluble in the aqueous media. Unfortunately, we cannot conclusively pinpoint where the pyrene partitions to on the basis of these viscosity correlations (i.e., whether the pyrene rests in a lipid environment or a peptide environment). Nonetheless, the assembled PA nanostructures present an internal solvation sphere and diffusional environment comparable to that of a moderately viscous solvent. They also offer an environment conducive to sequestering other molecules such as drug candidates and polymer precursors within the nanostructures.

Conclusions

We have used Stern−Volmer quenching studies to probe the interior of self-assembling peptide amphiphile cylindrical aggregates. Tryptophan PAs revealed that the peptide shell of these nanostructures remains well-solvated despite the physical location of the chromophore. Fluorescence quenching behavior of both covalently attached tryptophan and pyrene probes also indicated differential degrees of quencher penetration, where chromophores buried deeper within the aggregates showed a smaller response to aqueous quenchers relative to those located closer to the aggregate exterior. We compared these findings to a small molecule chromophore not covalently linked to the PA backbone that allowed for sequesteration from the aqueous environment after self-assembly. We found significant sequestration within these nanostructures along with sufficient solvation within them to allow for potential diffusion or release of molecules into the local environment. These studies help to demonstrate the potential of using PA nanostructures as carriers of hydrophobic molecules such as drugs, proteins, and small organic monomers.

Experimental Section

General Considerations. Preloaded Wang cross-linked polystyrene resins, Fmoc-protected amino acids, and 2-(1H-benzotriazole-1-yl)-1,1,3,3-tetramethyluronium hexafluorophosphate (HBTU) were purchased from NovaBiochem. Peptide synthesis grade *N*-methylpyrrolidone (NMP) was purchased from Fisher. All other reagents were purchased from Aldrich and used as received.

Automated peptide syntheses (Applied Biosystems 733A) were conducted on 0.25 mmol scales via standard Fmoc solid-phase synthesis on preloaded Wang resin supports (Fmoc deprotection: 30% (v/v) piperidine in NMP; Fmoc-protected amino acids were preactivated with HBTU and diisopropylethylamine (DIEA) in NMP prior to coupling). Final acylation of the resin-bound terminal amine was then conducted manually through HBTU/DIEA preactivation of palmitic acid in NMP (for **1**, **2**, and **6**) or of 1-pyrene butyric acid (for **3**). Reaction progress of manual couplings was monitored via ninhydrin staining. Cleavage of all PAs from the solid support was effected by agitation of the resin with a solution of trifluoroacetic acid (TFA), triisopropylsilane (TIS), water, and ethanedithiol (94:2:2:2) for 3 h, followed by filtration of the remaining resin and rinsing with TFA. Collected TFA solutions were then concentrated in vacuo and triturated with cold diethyl ether. The precipitates were filtered, rinsed with ether, and lyophilized prior to use.

Proton NMR (Inova Mercury 400) and matrix-assisted laser desorption ionization MALDI-TOF-MS (Voyager DE Pro) spectra were obtained at Northwestern University's Analytical Services Laboratory. MALDI measurements were obtained on α-cyano-4-hydroxycinnamic acid matrixes. **1**: calcd 1536.93, found 1537.14; **2**: calcd 1593.95, found 1594.52; **3**: calcd 1382.72, found 1382.14.

For **4** and **5**, we employed an orthogonal trityl protecting group (Mtt) on the desired lysine that could be selectively unveiled on the solid phase through treatment with 1% TFA and 5% TIS in CH_2Cl_2. In the synthesis of **4**, a Wang resin preloaded with Fmoc-protected glycine was deprotected manually (30% piperidine in NMP, 4 × 5 min) and rinsed (NMP, 5 × 5 min). Manual coupling of Fmoc-Lys(Mtt)-OH (activated by HBTU and DIEA in NMP) was repeated twice until judged complete by ninhydrin staining. Mtt deprotection (1% TFA as above, 5 × 5 min, followed by CH_2Cl_2 rinse 5 × 5 min) unveiled the free ϵ-amine. Pyrene acetic acid was then activated as described for pyrene butyric acid above and coupled to the free amine until no change was visible through ninhydrin resin testing. Acetic acid was similarly activated and added to the resin-bound peptide in order to cap any unreacted amines (<5%) to yield Wang resins functionalized with Gly-Lys(pyrene)-Fmoc. Automated synthesis of the remainder of the peptide and final *N*-acylation with palmitic acid provided the desired immobilized PA. Cleavage was effected as described above. MALDI: calcd for **4**, 1907.08; found, 1907.74.

The synthesis of **5** commenced from Wang-Val-Fmoc, followed by automated sequential addition of Ala-Val-Lys-Ile-Glu-Gly-Gly-Gly-Ala-Ala-Ala-Ala-NH_2. The final residue, Fmoc-Lys(Mtt)-OH, required manual double coupling to allow ninhydrin monitoring. Selective Mtt deprotection and acylation with pyrene acetic acid as described for **4** was followed by acetic acid capping of any unreacted lysine ϵ-amines. Final palmitic acid acylation and cleavage were performed as described above. MALDI: calcd for **5**, 1721.02; found, 1722.5.

Spectroscopy. Stock solutions of PAs were prepared at high pH (ca. 10) at 1 mg/mL in degassed MilliPore water, filtered through a 0.45 μm filter, and diluted to micromolar concentrations to ensure optical densities less than 0.05. These dilute solutions were then acidified to pH 2 in order to mimic self-assembling conditions. We found similar trends when separate PA stock solutions were acidified to pH 2, immediately sonicated for a minute and vortexed to suppress extensive aggregation, and diluted to identical micromolar concentra-

tions. UV−vis measurements were taken on a Cary 500 UV−vis−NIR spectrometer in the Keck Biophysics Facility at Northwestern University, and steady-state fluorescence measurements were taken on an ISS PC1 fluorometer by excitation at 290−295 nm (for **1** and **2**) or 340−345 nm (for **3**−**5**) using a Xenon arc lamp light source. Emission spectra for **1** and **2** were collected through a 305-nm cut-on filter to eliminate tails from Raman scattering. Aqueous acrylamide (8 M) was added in small aliquots as to not dramatically affect the chromophore concentration. Fluorescence intensities were corrected for instrument response and inner filter effects arising from acrylamide absorption at the excitation wavelength (for **1** and **2**). Fluorescence lifetime measurements were obtained through phase-modulation techniques on an ISS K2 fluorometer at the excitation wavelengths listed above. Reported lifetimes were measured vs LUDOX scattering solution, and these values were consistent with small molecule lifetime standards, with or without magic-angle polarizer orientations. Cut-on filters were also used to minimize contributions from scattering (305 nm for **1** and **2**, 375 nm for **3**−**5**). Circular dichroism measurements were conducted on PA solutions with concentrations of ca. 3.8×10^{-6} M at the Keck Biophysics Facility (Jasco J-715).

Microscopy. Transmission electron microscopy was performed on a Hitachi H8100 operating at 200 kV in the Electron Probe Instrumentation Center at Northwestern University. All samples were prepared on copper grids (coated with holey carbon) by direct submersion in 1 wt % self-supporting hydrogels of the desired PA system. For co-assembled systems, the gels were prepared at 1 wt % of the diluent **6** in addition to maintaining a 40-fold excess of **6** with respect to the fluorescent PA (**3**−**5**). Following exposure to the gels, all sample grids were rinsed with water, wicked dry, stained with phosphotungstic acid (2% in water) for 30 s, and wicked dry.

Acknowledgment. Generous financial support of this research was provided by the DOE (Grant DE-FG02-00ER45810). J.D.T. thanks Baxter Healthcare and the Institute for BioNanotechnology in Medicine (IBNAM) at Northwestern University for postdoctoral support as a recipient of the Early Career Development Award. We thank Krista L. Niece and Lorraine Hsu for automated peptide syntheses, Dr. Jack J. J. M. Donners for graphics of PA self-assembly, and Dr. Liang-shi Li for advice with TEM acquisition. We gratefully acknowledge the use of instruments in the Keck Biophysics Facility, the Electron Probe Instrumentation Center, and the Analytical Services Laboratory at Northwestern University.

Supporting Information Available: NMR spectra of PAs **1**−**5**, CD, UV−vis, and fluorescence spectra of **1**, **2**, and 1:40 solutions of **3**, **4**, and **5** with **6** in the absence of aqueous quenchers, UV−vis and fluorescence for 1:40 solutions of pyrene acetic acid with PA **6**, TEM images of all PAs studied (**1** and **2** as well as the 1:40 coassemblies, **3:6**, **4:6**, **5:6**), regular Stern−Volmer plots for 1:40 coassemblies of pyrene PAs **3**, **4**, and **5** with diluent PA **6**. This material is available free of charge via the Internet at http://pubs.acs.org.

JA043764D